ACS APPLIED BIO MATERIALS
Cite This: ACS Appl. Bio Mater. 2019, 2, 2125−2136
Article
www.acsabm.org

Detection of the Enzymatic Cleavage of DNA through Supramolecular Chiral Induction to a Cationic Polythiophene

Mathieu Fosséprés,[†,‡] Marie E. Trévisan,[†,‡] Valentine Cyriaque,[§] Ruddy Wattiez,[§] David Beljonne,[‡] Sébastien Richeter,[⊥] Sébastien Clément,[⊥] and Mathieu Surin*[,‡]

[‡]Laboratory for Chemistry of Novel Materials, Centre of Innovation and Research in Materials and Polymers (CIRMAP), University of Mons (UMONS), 20 Place du Parc, Mons B-7000, Belgium

[§]Proteomics and Microbiology Lab, Research Institute for Biosciences, University of Mons (UMONS), Avenue du Champs de Mars 6, Mons 7000, Belgium

[⊥]Institut Charles Gerhardt ICGM, UMR 5253 CNRS-ENSCM-UM, Université de Montpellier, CC1701 Place Eugène Bataillon, Montpellier Cedex 05F-34095, France

Supporting Information

ABSTRACT: Water-soluble π-conjugated polymers are increasingly envisioned in biosensors, in which their unique optical and electronic properties permit a highly sensitive detection of biomolecular targets. In particular, cationic π-conjugated polymers are attractive for DNA sensing technologies, through the use of the fluorescence signals either in physiological solutions or in thin films. However, in the context of enzymatic activity assays, fluorescence-based methods require covalently labeling DNA with a dye or an antibody and are limited to short time scale due to dye photobleaching. In this frame, we report here a novel possible approach to probe the cleavage of DNA by a restriction enzyme, in continuous and without covalently labeled DNA substrate. This is achieved by exploiting unique chiroptical signals arising from the chiral induction of DNA to a poly[3-(6′-(trimethylphosphonium)-hexyl)thiophene-2,5-diyl] upon interaction. The cleavage of DNA by *Hpa*I, an endonuclease enzyme, is monitored through circular dichroism (CD) signals in the spectral range where the polymer absorbs light, i.e., far away from the spectral ranges of both DNA and the enzyme. We compare the results to a conventional noncontinuous assay by polyacrylamide gel electrophoresis, and we demonstrate that induced CD signals are effective in probing the enzymatic activity. By means of molecular dynamics simulations and calculations of CD spectra, we bring molecular insights into the structure of DNA/polymer supramolecular complexes before and after the cleavage of DNA. We show that the cleavage of DNA modifies the dynamics and the organization of the polymer backbone induced by the DNA helix. Altogether, our results provide detailed spectroscopic and structural insights into the enzymatic cleavage of DNA in interaction with a π-conjugated polymer, which could be helpful for developing chiroptical detection tools to monitor the catalytic activity in real time.

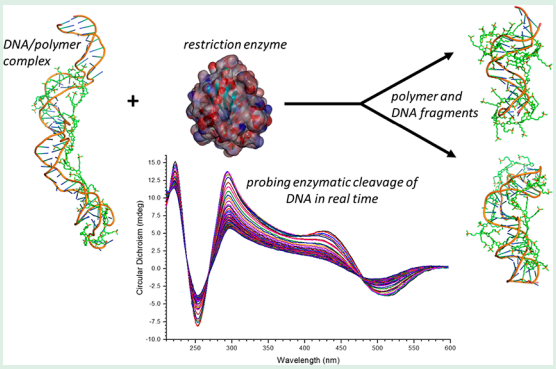

KEYWORDS: *DNA, enzymatic assay, polythiophene, chiral induction, circular dichroism, molecular modeling*

INTRODUCTION

The design of biosensors has become more and more important because of the need to offer rapid and sensitive detection methods.[1,2] For instance, biosensors have been developed for the analysis of contaminants in environmental science, for early detection and diagnosis in medicine, and for the detection of specific analytes for food quality control.[1−8] Many research efforts have also been devoted to developing detection tools for genetics and genomics, for example, for accurate determination of DNA concentration, sequence analyses, and detection of single-nucleotide variations.[8−11] Currently, there is an important need to detect enzymatic activity toward DNA, as a key issue for understanding the genetic integrity and regulation, and develop DNA-based enzyme-responsive materials.[12−16] Many enzymes are at play to separate DNA strands, cleave DNA, repair DNA, transfer specific groups on nucleobases, or transpose DNA fragments, and these chemical modifications of the genetic material are key in the regulatory functions.[13,17−20] The detection of the enzymatic activity toward DNA is crucial to reveal the kinetics of enzymes with various substrates, and to assess thermodynamic data such as the affinity of enzyme inhibitors, cofactors, and activators.[21] To explore the enzymatic activity, researchers have developed assays based on electrophoresis, chromatog-

Received: February 14, 2019
Accepted: April 1, 2019
Published: April 1, 2019

DOI: 10.1021/acsabm.9b00123
ACS Appl. Bio Mater. 2019, 2, 2125−2136

Scheme 1. Chemical Structure of the Cationic Conjugated Polymer (Left) and DNA Sequence under Study (Right)[a]

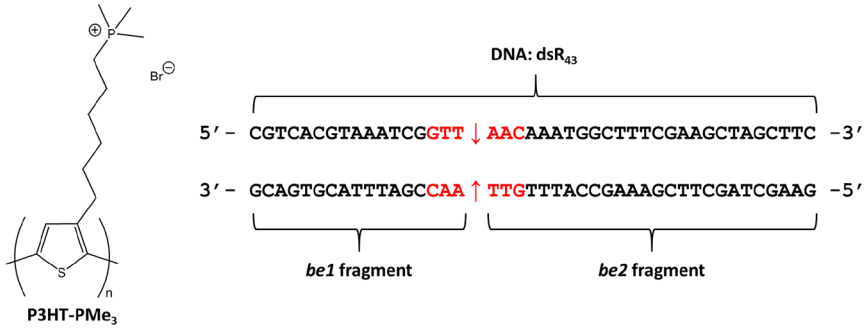

[a]The specific restriction site of *HpaI* is depicted in red, with arrows pointing to the cleavage site.

raphy, calorimetry, mass spectrometry, etc. However, most of these enzymatic assays are time-consuming or noncontinuous or suffer from the necessity of labeling DNA with radioactive elements. Fluorescence is also largely used as a convenient optical method to monitor enzyme activity toward DNA.[22−24] However, the covalent attachment of fluorescent dyes on DNA involves chemical modifications of DNA, and the activity as well as the specificity of the enzymes can be affected, and the assays may be altered by dye photobleaching. Therefore, new methods to monitor the enzymatic activity in real-time and without covalent labeling are needed.

One of the strategies to develop these detection tools is to explore supramolecular approaches that make use of electrostatic interactions between cationic molecules and the anionic phosphodiester backbone of DNA.[25,26] In this frame, water-soluble π-conjugated polymers are promising transducers for signaling the recognition of biomolecules and their reactivity in regards to their unique optical and electronic properties.[7−9,27−33] For genomic applications, cationic π-conjugated polyelectrolytes (CPEs) were reported to strongly interact with DNA in aqueous solution, which was exploited to probe DNA lesions or single-nucleotide polymorphisms at very low DNA concentrations.[8,27,29,34−38] The detection of enzymatic activity toward DNA based on π-conjugated molecular probes constitute an emerging topic.[39−41] Up to now, this detection has been achieved mostly through the use of Förster resonance energy transfer (FRET) between a π-conjugated polymer and a dye-labeled DNA, with FRET ratio related to enzymatic activity, e.g., for a kinase or a methyltransferase.[41−43] Besides, George and some of us reported the use of circular dichroism (CD) signals of supramolecular polymers (made of naphthalenediimide derivatives functionalized with Zn^{2+} complexes) binding adenosine triphosphate (ATP) to monitor the activity of a phosphatase in real-time.[44] We showed that the evolution of CD signals reflect the extent of ATP hydrolysis by the phosphatase, going from supramolecular polymers bound to ATP, to ADP, then AMP, and eventually phosphates. Indeed, CD signals are very sensitive to changes in the microenvironment and were shown to be effective in studying supramolecular systems,[45,46] in particular for supramolecular DNA recognition.[47−49]

Tempted to apply this supramolecular approach to further probe the enzymatic activity with DNA as substrate in real-time through chiroptical signals, we figured out that a cationic π-conjugated polymer could be exploited to interact with the anionic phosphodiester backbone along DNA. We selected poly[3-(6′-(trimethylphosphonium)hexyl)thiophene-2,5-diyl] (P3HT-PMe_3, see Scheme 1), an achiral polymer that showed intense induced CD signals when interacting with DNA.[50,51] This polymer was notably exploited by us for the detection of single-nucleotide polymorphism in DNA−DNA hybridization experiments.[52] From previous studies, we observed that this polymer is preferentially adsorbed along DNA minor grooves, therefore possibly not too much hampering an enzyme that functions in the DNA major grooves. In the present study, we show that this cationic π-conjugated polymer can be used to probe the cleavage of DNA by *Hpa*I, an endonuclease enzyme issued from the microorganism called *Haemophilus parainfluenzae*, cleaving double-stranded DNA in blunt ends. For this, P3HT-PMe_3 is complexed with a 43-base-pair DNA (dsR43) containing a specific restriction site of *Hpa*I, i.e., 5′---GTTAAC---3′, becoming 5′---GTT and AAC---3′ after the cleavage (Scheme 1).[52] The double-stranded DNA dsR_{43} is cleaved in two blunt-end (be) DNA fragments, namely be1 and be2 (Scheme 1). By exploiting induced circular dichroism (ICD) signals in the spectral range where the achiral polymer absorbs (400−600 nm), i.e., far away from the UV region where both the enzyme and DNA absorb (in the UV, up to 300 nm), we interrogate the pertinence of cationic π-conjugated polymers as probes to follow enzymatic activity throughout ICD techniques. As the ICD signals of DNA/P3HT-PMe_3 complexes are sensitive to the DNA sequence, the appearance of ICD signals related to complexes with the be1 and be2 fragments could be monitored throughout time as an indication of *Hpa*I activity.

In this paper, we first report on the complexation between dsR_{43} and P3HT-PMe_3, by means of UV−vis absorption and CD spectroscopies. Molecular dynamics (MD) simulations are used to investigate the assembly, the dynamics, and the effect of chiral induction in the DNA/polymer complexes. Next, we assess the effect of addition of *Hpa*I, catalyzing the cleavage of dsR_{43} in two fragments, on the CD signals in a continuous manner. The evolution of these signals is compared to the extent of enzymatic activity estimated through a non-continuous assay by gel electrophoresis. Finally, we evaluate the differences in spectroscopic signals and in the structure/dynamics of the complexes according to the size of the DNA fragments. By combining MD simulations with calculations of CD spectra, we reveal the conformational changes of the polymer chain depending on the DNA length in the complex. The combination of CD, gel electrophoresis, and molecular modeling points to the usefulness of DNA/CPE supramolecular assemblies to track the activity of an enzyme throughout time.

DOI: 10.1021/acsabm.9b00123
ACS Appl. Bio Mater. 2019, 2, 2125−2136

EXPERIMENTAL DETAILS

Materials and Sample Preparation. Oligonucleotides (ODN) dsR_{43} and dsR_{20} (Scheme 1 and Table S1) were purchased at the highest purity grade (UltraPureGold from Eurogentec, Belgium). Stock solution at 100 μM were prepared in Milli-Q water and stocked at −18 °C. P3HT-PMe_3 was synthesized as previously described,[51,53] and a stock solution of P3HT-PMe_3 was prepared at 200 μM in Milli-Q water. Samples of endonuclease *Hpa*I and its restriction buffer (Cut Smart Buffer 10x) were purchased from New England Biolabs (NEB). *Hpa*I was provided in Cut Smart Buffer 1x (CSB1x, pH 7.9 at 293 K), composed of 20 mmol L^{-1} Tris-acetate; 10 mmol L^{-1} magnesium acetate; 50 mmol L^{-1} potassium acetate and 100 $\mu g.mL^{-1}$ Bovine Serum Albumin. For the separation of gel electrophoresis, 1L of TBE (Tris-Borate-EDTA) 10× was prepared as well as an aqueous STOP buffer composed of 60% (w:w) sucrose and 500 mmol L^{-1} EDTA. GelRed provided by Biotium was used as DNA stain. All experiments were performed at 37 °C.

For the titration experiments, a small volume (5−10 μL) of stock solution of ODNs was diluted in 300 μL of 1× CutSmart buffer until the absorbance at 260 nm reached 0.7 A.U. dsR20 samples were two times more concentrated than dsR43 samples to have a similar charge ratio in the mixture. Solutions of P3HT-PMe_3 and ODN (to cancel dilution effects and maintain a constant concentration in DNA) were then added in the solution to obtain the working [ODN]:[P3HT-PMe_3] molar ratios. For the enzymatic cleavage experiments, solutions of 1:2 molar ratio in dsR43:P3HT-PMe_3 were prepared in CSB1×, and 3 units of *Hpa*I per μg of ODN were added to the mixture (CD-mix). For the CD control experiment (CD-control), the volume of *Hpa*I was replaced by the same volume of buffer.

For the gel electrophoresis experiments, one sample (called GE-mix) was prepared as described above for cleavage, the other was used as control (called GE-control) and prepared by diluting dsR_{43} in 300 μL of 1× CutSmart buffer until the absorbance at 260 nm reached 0.7 A.U, then 3 units of *Hpa*I per μg of ODN were added to the sample. Five microliters of GE-control mixture were extracted every 5 min for 1.5 h. The collected volume was added to an Eppendorf containing 2.5 μL of 6× purple loading gel dye and 2 μL of STOP buffer and immediately iced. Ten microliters of GE-control mixture were extracted every 6 min for 3 h. The collected volume was added to an Eppendorf containing 5 μL of loading gel dye purple 6× and 4 μL of STOP buffer and immediately iced. All samples were stored at −18 °C until gel electrophoresis.

(Chir)optical Spectroscopy. UV−vis absorption and CD spectra were recorded with a ChirascanPlus CD spectrophotometer (from Applied Photophysics). Measurements were performed on samples in 2 mm path length quartz Suprasil cuvettes, with a bandwidth and step of 1 nm and with a time per point of 0.5 s. All experiments were performed in 1× CutSmart buffer at 37 °C, using a TC125 temperature controller from Quantum Northwestern running on the spectrophotometer and the temperature within the cuvettes was determined using a temperature probe.

Polyacrylamide Gel Electrophoresis. Gel electrophoresis was performed on a 20% polyacrylamide gel with TBE 1× buffer at 298 K. Gel ran in a BIO RAD DcodeTM vat with a constant voltage of 75 V, an intensity of 10 mA and power of 1 W for 4 h for the GE-control samples and 14 h for the GE-mix samples. Gels were stained with 0.0005% GelRed for 30 min then pictures were taken with a 3 s exposure time using UV illumination Gel Doc 2000. Gel pictures were analyzed with ImageJ. The areas of the intensity peaks of PAGE bands were estimated from the plots of lanes with ImageJ, and then normalized by the total intensity.

THEORETICAL DETAILS

Molecular Dynamics (MD) simulations were performed to study the early stages of the self-assembly between P3HT-PMe_3 and double-stranded DNA. MD simulations involve both the assembly between P3HT-PMe_3 and dsR_{43} DNA, and between P3HT-PMe_3 and each of the two DNA fragments that issued from *Hpa*I activity on dsR_{43}, i.e., the be1 and be2 DNA fragments. The starting B-DNA conformations were built within the NAB (Nucleic Acid Builder) AmberTools16 module.[54] The starting conformations of P3HT-PMe_3 were built within the LEaP program, the molecular builder module of AMBER16.[52] For the three systems, P3HT-PMe_3 was oriented in a perpendicular way of the DNA helix axis to avoid any bias of the polymer preorientation with DNA. The starting interdistance between the DNA and P3HT-PMe_3 was superior to 15 Å to prevent any bias of the DNA/CPT recognition mode due to initial intermolecular interactions before the MD simulations. The three starting systems are depicted in the Figure S1. A MD simulation of P3HT-PMe_3 was performed in order to study the intrinsic dynamics of the polymer. All simulations were achieved with the AMBER16 package. The parmBSC1 force field (FF) was used to consider DNA dynamics,[55] and GAFF 2.1 FF was employed for the polymer.[56] A reparameterization of the bithiophene torsion potential estimated at the MP2/cc-pvdz level and charge calculations were performed as described in ref 34. An appropriate number of counterions were added to neutralize the net charge of the molecular systems, i.e., 37 Na^+ counterions for the dsR43/P3HT-PMe_3 system, 15 Cl^- counterions for the be1/P3HT-PMe_3 system, and 3 Na^+ counterions for the be2/P3HT-PMe_3 system. To conduct a relevant conformational sampling on the microsecond time scale, the MD simulations were performed in an implicit solvent using the generalized Born solvation model.[57] For the three systems, the same MD protocol in three steps (minimization-heating/equilibration-production) was applied. A first minimization was performed to relax the ionic atmosphere of the molecular systems. For this, a steepest descent minimization of 1000 steps was carried out with harmonic positional constraints applied to the DNA and the CPT with a force constant of 25 kcal mol^{-1} $Å^{-2}$, followed by a conjugate gradient minimization in 9000 steps. A second minimization of 10 000 steps (1000 steepest descent steps followed by 9000 conjugate gradient steps) was carried out without any restraints on the molecular systems. The heating-equilibration stage was then performed for 2 ns in the NVT ensemble. A 2 fs time step was used as the SHAKE algorithm constrained the length of covalent bonds that involved hydrogen atoms. Harmonic positional constraints were applied to DNA and P3HT-PMe_3 with a force constant of 10.0 kcal mol^{-1} $Å^{-2}$ to avoid any deformation of DNA or P3HT-PMe_3 during the heating process. First, the system was heated from 0 to 300 K over 1 ns. The temperature was then maintained for another 1 ns with the Langevin thermostat and a collision frequency of 1.0 ps^{-1}. Finally, the MD production stage was performed for a simulation time of 1.5 μs. During the production stage, a 2 fs time step was employed with the Langevin thermostat with a 1.0 ps^{-1} collision frequency. MD snapshots were recorded each 0.5 ns, resulting in a 3,000 frames trajectory at the end of the production MD. Extraction of MD snapshots and trajectory analyses were done with the CPPTRAJ AmberTool16 module. Statistical analyses on the MD trajectories were carried out with the R package.[58] Images of the MD snapshots were rendered with PyMOL 2.2.0.[59] To gain insight into the origin for the chiral response of the P3HT-PMe_3 interacting with DNA, we solved a simple Frenkel exciton model including both through-space and through-bond interactions between the thiophene monomer units of the P3HT-PMe_3. CD spectra were then simulated on the basis of

DOI: 10.1021/acsabm.9b00123
ACS Appl. Bio Mater. 2019, 2, 2125−2136

the calculated rotational strengths from the ground state to the excitonic state manifold. Results of the model were validated against semiempirical quantum-chemical excited-state calculations performed on selected frames. Details about the computational approach are provided in the Supporting Information.

RESULTS AND DISCUSSION

Chiroptical Signals and Supramolecular Assembly of dsR_{43}/P3HT-PMe_3. UV−vis absorption and CD spectroscopies are carried out on buffered aqueous mixtures of dsR_{43}/P3HT-PMe_3, with a particular focus on ICD signals, i.e., CD signals in the range where P3HT-PMe_3 absorbs. These ICD signals were previously observed quite sensitive to the DNA length and sequence.[50,51] Titrations experiments of dsR_{43} by the polymer are performed at 37 °C, see Figure 1. In the DNA

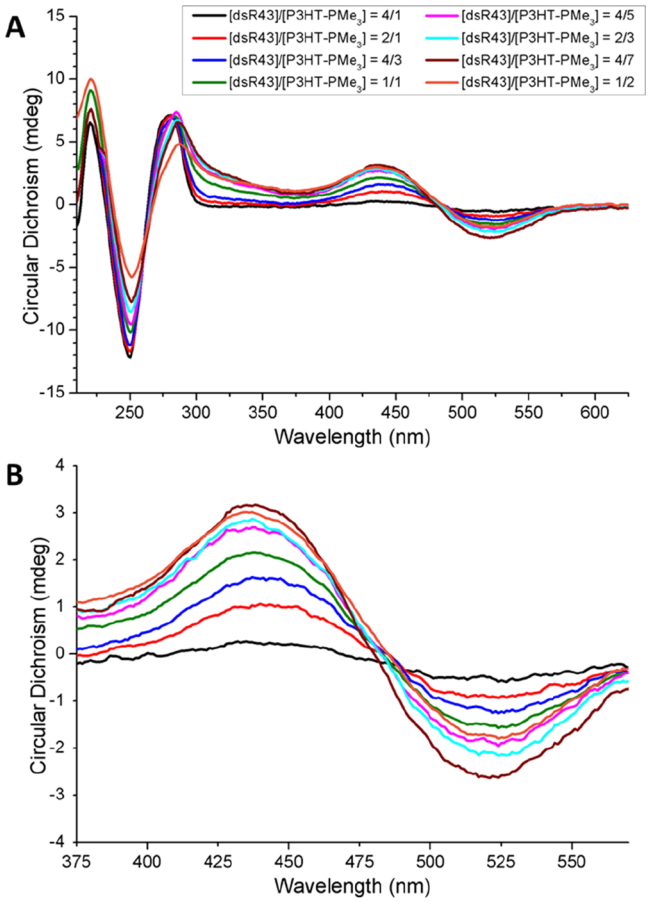

Figure 1. (A) Circular dichroism (CD) spectra of dsR_{43}/P3HT-PMe_3 mixtures in CSB1× buffer at 37 °C, at different molar ratios (concentration of dsR_{43} = 5 μM). (B) Zoom on the induced CD signals in the spectral range of P3HT-PMe_3.

absorption range (240−280 nm, Figure 1A), the CD signals are slightly decreasing upon addition of P3HT-PMe_3, although the concentration of DNA in solution is maintained constant. A bisignate (−/+) ICD signal appears in the polymer main absorption in the visible range (Figure 1), as a signature of the induced chirality from the chiral DNA to the achiral polymer upon interaction. It is intriguing that this ICD signature is (−/+), i.e. that of a left-handed polythiophene chain (or assembly), whereas the double-stranded DNA is indeed a right-handed helix in our conditions. This is rationalized by calculations of CD spectra based on molecular modeling simulations (see below). Further addition of P3HT-PMe_3 (at a constant concentration in DNA) leads to more intense ICD signals, with saturation around a molar ratio of 1:2 in dsR_{43}:P3HT-PMe_3 (Figure 1B), corresponding to an approximate charge ratio of 1:1, above which aggregation is observed. Note that UV−vis spectra of mixtures indicates a large red-shift of the main absorption band of the pure polymer (λ_{max} = 443 nm) compared to dsR_{43}:P3HT-PMe_3 mixtures (λ_{max} = 473 nm at 1:1 molar ratio, Figure S2); this shift is attributed to a partial planarization of the polymer backbone upon DNA binding.[29,50,51]

To understand the supramolecular assembly of dsR_{43} with P3HT-PMe_3 and the DNA-induced chirality of the polythiophene chains, we carried out MD simulations, as these were shown to be effective at providing molecular details in the early steps of the complexation between π-conjugated molecules and biomolecules.[34,50,60−63] From MD simulations of 1:1 complexes on a 1.5 μs time scale (starting from perpendicular orientation of DNA and polymer chains, to avoid any bias), the anionic dsR_{43} and cationic P3HT-PMe_3 rapidly forms a complex with various levels of organization, as shown in Figure 2 depicting several snapshots along the MD simulation. The complexation between dsR_{43} and P3HT-PMe_3 is a fast process occurring on the nanosecond time scale in our MD simulation. The interdistance between the centers of masses of dsR43 and P3HT-PMe_3 macromolecules rapidly decreases from more than 10 to 5 Å during the first 10 ns of the MD production (Figure S3). With an average value of around 8 Å and a standard deviation of only 0.8 Å, no important variation of the interdistance is observed during the rest of the MD simulation, meaning that the dsR_{43}/P3HT-PMe_3 complex is stable over the microsecond time scale. MD simulations also reveal a significant conformational reorganization of the chains with time, see the variation of the RMSD with time (Figure 2A). During the first nanoseconds of the MD simulation, the RMSD profile of dsR_{43} is rapidly going up to a plateau related to the RMSD average value, i.e., around 16 Å. A non-negligible standard deviation of 1.9 Å and the presence of RMSD peaks indicates that the DNA undergoes large conformational dynamics once the complex is formed. The RMSD variation comes from the ability of the dsR_{43} to be intrinsically curved along its double-helix axis (see MD snapshots in Figure 2), this DNA bending being driven by the strong electrostatic interactions between DNA and P3HT-PMe_3.

In parallel, P3HT-PMe_3 also undergoes a large conformational reorganization in the beginning of the MD simulation. We observe a rapid increase of the P3HT-PMe_3 RMSD profile (average RMSD, 15 Å; maximum RMSD, ∼19 Å), as shown in Figure 2A. On the other hand, the RMSD standard deviation is only 0.8 Å. The P3HT-PMe_3 is less flexible than dsR_{43} once associated with the DNA fragment. The MD snapshots in Figure 2 show that the P3HT-PMe_3 adopts a specific organization that consists in a relatively linear, twisted conformation along the DNA helix. As a consequence, the end-to-end distance of P3HT-PMe_3 is small in respect to the size of the polymer. The end-to-end distance profile of P3HT-PMe_3 (Figure 2B) has an average value of ∼64 Å (standard deviation ∼5 Å), far from the end-to-end distance of the completely extended starting conformation (∼180 Å). By contrast, MD simulations of the polymer in absence of DNA (Figure 2B) show higher average end-to-end distance (144 Å)

DOI: 10.1021/acsabm.9b00123
ACS Appl. Bio Mater. 2019, 2, 2125−2136

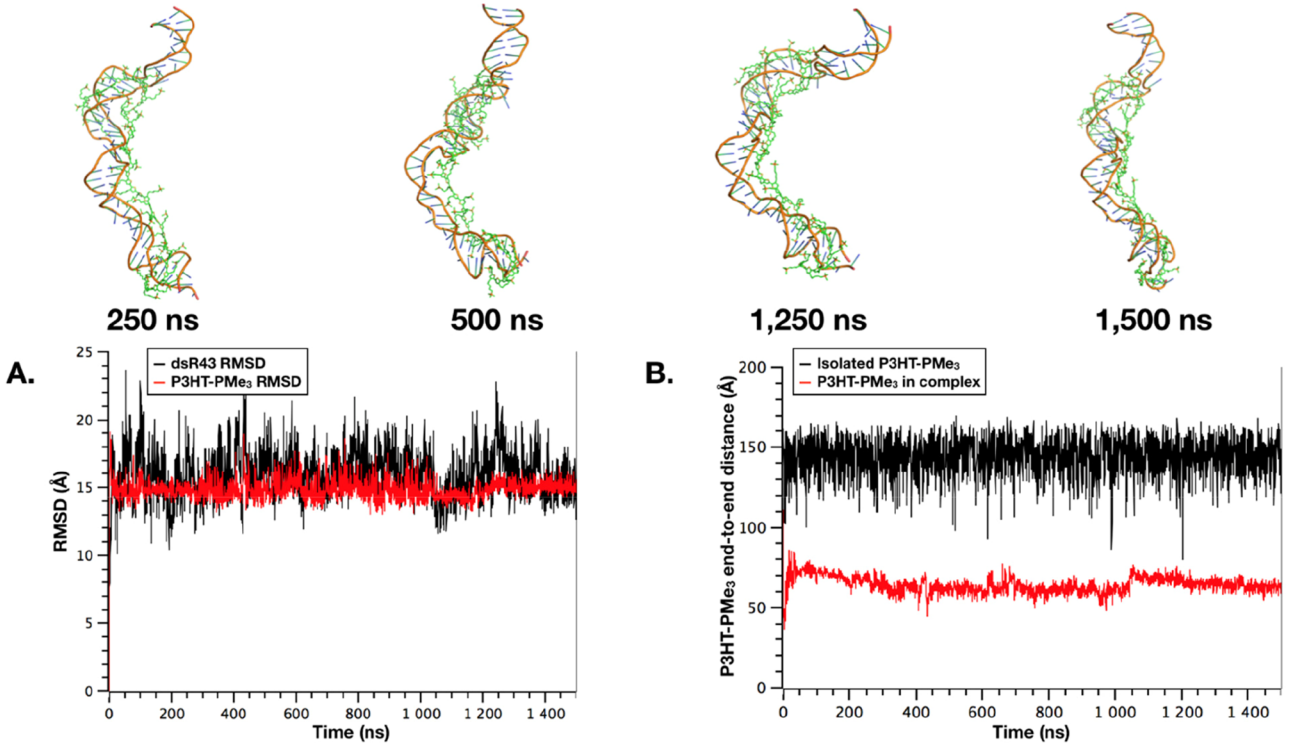

Figure 2. Top: Snapshots extracted from MD simulations of the assembly between P3HT-PMe_3 (in green) and dsR_{43} (in orange and blue). Cartoon representations were used for DNA; for clarity, hydrogen atoms of P3HT-PMe_3 were omitted. Bottom: (A) Root-mean-square deviations (RMSD) of dsR_{43} and P3HT-PMe_3, calculated according to the first conformation of the MD production phase. (B) Profiles of the end-to-end distances for MD simulations of P3HT-PMe_3 alone and in complex with DNA. The end-to-end distances were calculated between the first and last sulfur atoms along the polymer sequence.

as well as a large standard deviation (11 Å). Let us note that the linearity of P3HT-PMe_3 is however limited when complexed with dsR43. The polymer is wrapped around the DNA double helix, as depicted for each snapshot reported in Figure 2A.

The profiles of dihedral angles between thiophene units along the polymer backbone are estimated as a fingerprint of the conformations (Figure S4). The P3HT-PMe_3 dihedral angle profiles of a series of MD snapshots, recorded each 250 ns, are then compared in a consecutive way with reference to the previous one. Correlation coefficients between the P3HT-PMe_3 dihedral profiles (Table 1) in the complex increase along the simulation, to reach very high values (0.90, with a peak of 0.97) for the last half of the MD run. On the contrary, the similarity between the dihedral profiles of the isolated P3HT-PMe_3 remains below 0.80, although it is raising with time with the stabilization of the polymer (Table 1). The calculation of the similarity between the P3HT-PMe_3 dihedral profiles on a smaller time scale, i.e. between consecutive MD snapshots recorded each 125 ns, leads to similar conclusions (Table S2). This shows that the polymer adopts a limited range of conformations upon assembly with DNA. Hence, the limited flexibility, the linear and twisted conformation of P3HT-PMe_3, consequent to the organization of the polymer along the DNA helix, involve a convergence of the P3HT-PMe_3 dihedral profiles. The analysis of MD in the time scale between 1.0 and 1.5 μs, i.e. where these correlation coefficients were high (>0.90), shows mostly left-handed conformations of the polythiophene chain, as revealed by numerical simulations of CD spectra (see below).

Table 1. Correlation Coefficients (CC) of P3HT-PMe_3 Dihedral Profiles[a]

time (ns)	CC of P3HT-PMe_3 (alone) dihedral profiles	CC of P3HT-PMe_3 (in complex) dihedral profiles
250	0.12	0.18
500	0.12	0.60
750	0.46	0.93
1000	0.60	0.97
1250	0.76	0.91
1500	0.80	0.95
average	0.48	0.76

[a]CC was calculated between consecutive snapshots recorded each 250 ns for P3HT-PMe_3 both alone and in complex with DNA.

Cleavage of DNA in Supramolecular Assemblies of dsR_{43}/P3HT-PMe_3. The evolution of CD signals upon the addition of *Hpa*I (3 units per μg of DNA) onto a mixture of dsR_{43}:P3HT-PMe_3 (1:1 charge ratio) in the enzyme buffer is monitored, with up to 50 successive CD spectra (up to ~5 h). The results of this experiment, called CD-mix, are shown in Figure 3. In the range where the polymer absorbs, we observe a continuous decrease of CD intensities with time (Figure 3B, C), together with blue-shifts of these ICD signals (Figure 3C, D). We also monitor a control experiment (CD-control), for which we add a buffer solution without the enzyme, in an equal volume. From the comparison, we observe a decrease of the intensity of ICD signals in both experiments, which we attribute to a partial aggregation of the complexes upon addition of the enzyme buffer (Figure S5). However, the global evolution of the ICD signals is quite different for the enzymatic assay and the control experiment (i.e., without enzyme). For

DOI: 10.1021/acsabm.9b00123
ACS Appl. Bio Mater. 2019, 2, 2125−2136

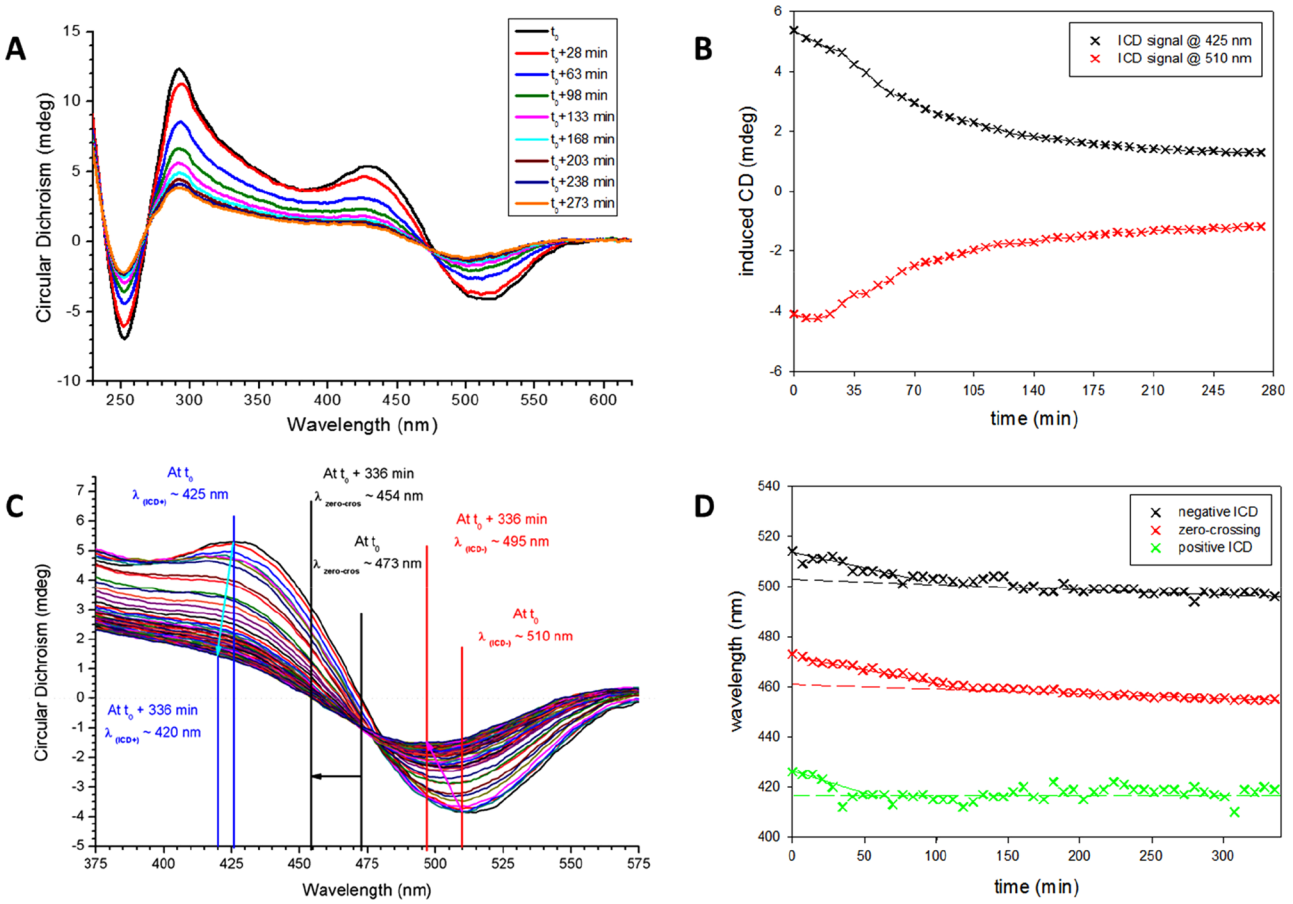

Figure 3. (A) Time evolution of CD spectra of dsR_{43} + P3HT-PMe_3 complexes in CSB1x buffer at 37 °C upon addition of 3 units of *Hpa*I enzyme per μg of DNA (by convention, the enzyme is added at t_0). (B) Evolution of the CD intensities of the positive ICD signal (black crosses) and negative ICD signal (red crosses) with time. (C) Closer inspection of the induced CD signals in the P3HT-PMe_3 absorption range with time. (D) Evolution of λ_{max} for ICD signals shown in C as a function of time.

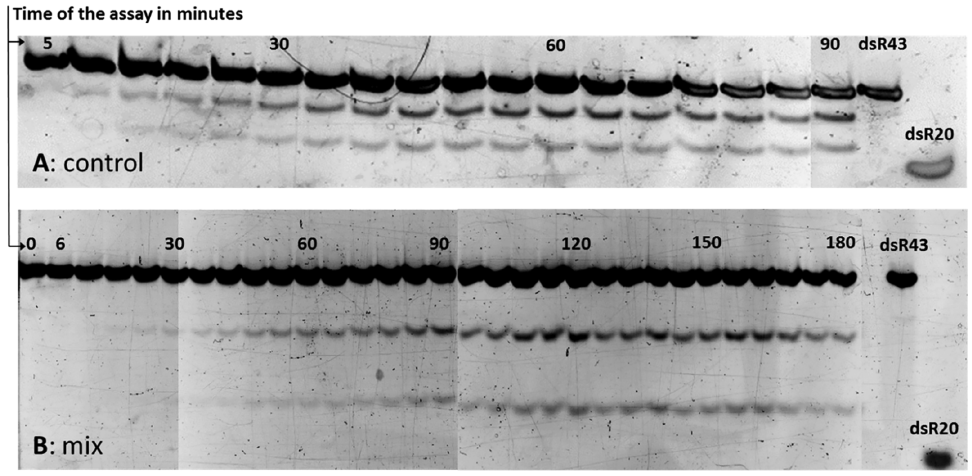

Figure 4. Polyacrylamide gel electrophoresis as revealed by fluorescence, displaying the cleavage of dsR_{43} into dsR_{17} (be1) and dsR_{26} (be2) fragments over time from the left to the right. (A) Enzymatic assay for the control experiment (GE-control: dsR_{43} + *Hpa*I). (B) Enzymatic assay with the cationic polythiophene (GE-mix: dsR_{43} + P3HT-PMe_3 + *Hpa*I). The last two lanes on the right of the gels contain dsR_{43} and dsR_{20} used as references.

the control experiment (CD-control, in Figure S5A), we observe that the position of the negative ICD signal (i.e., below zero in CD intensity) remains stable with a maximum ICD around 505 nm upon addition of the buffer. The zero-crossing at 470 nm very slightly shifts of a few nm, while the positive ICD signal (i.e., above zero in CD intensity) below 425 nm remains stable in terms of band position. In contrast, for experiments with the *Hpa*I enzyme (CD-mix, Figure 3 and Figure S5B), we observe a progressive blue-shift of all components of the ICD signal with time (Figure 3C, D): a

DOI: 10.1021/acsabm.9b00123
ACS Appl. Bio Mater. 2019, 2, 2125−2136

large shift of the zero-crossing of $\Delta\lambda \approx -20$ nm (highlighted by vertical black lines in Figure 3C), a shift of $\Delta\lambda \approx -5$ nm for the positive ICD signal at 425 nm, and a shift of $\Delta\lambda = -15$ nm for the negative ICD signal at 510 nm (see Figure 3C). Note that the positive ICD signal flattens with time, thus rendering difficult the determination of maximum ICD wavelength. By charting the evolution of the wavelengths for the different parts of the ICD signals with time (Figure 3D), we observe that the evolution of the CD signals follows first a steep decrease from a few minutes up to a change of slope appearing between 70 min and around 100 min (depending on the ICD signal), after which the ICD signals remain constant or only slightly decrease with time (dashed line). This discontinuity at around 70−100 min is also found in the repeats (Figure S6). This could also be observed when monitoring the change in the λ_{max} of the polymer in UV−vis absorption spectra, which shows a discontinuous decrease in the polymer λ_{max} that spans from a few minutes to around 100 min (Figure S7). We hypothesize that these changes of slopes in the spectroscopic signals with time are the signatures of the enzymatic activity.

To verify our hypothesis, we perform enzymatic assays by conventional polyacrylamide gel electrophoresis (PAGE) on the mixture dsR_{43}/P3HT-PMe_3 + *Hpa*I (called GE-mix) and on a control assay dsR_{43} + *Hpa*I (called GE-control), see Figure 4. These two assays are performed in the same conditions as the CD assays. The positive control shows that DNA fragments issued from cleavage are visible on the gel 5 min after addition of *Hpa*I (Figure 4A and Figure S8). Normalized areas of the intensity peaks of PAGE bands are shown over time in Figure 5. For the GE-control experiment (Figure 5A), the area of these peaks corresponding to the cleft DNAs, dsR_{17} (be1) and dsR_{26} (be2), increases until around 60 min, after which it reaches a plateau. At this plateau, the band intensities of dsR_{17} and dsR_{26} fragments represent around 30% of the total intensity. The analysis of the gel GE-mix (i.e., dsR_{43} + P3HT-PMe_3 + *Hpa*I) shows that fragments issued from cleavage are visible on the gel beyond the third band (i.e., 18 min) after addition of *Hpa*I (at time 0 by convention), see Figure 4 and Figure 5B. The normalized areas corresponding to DNA fragments increase until reaching a plateau after around 90 min, where the intensity of the fragments be1 and be2 represent around 30% of the total intensity. Indeed, PAGE indicates that P3HT-PMe_3 inhibits the enzymatic activity, but does not stop it. The presence of the polymer hinders the start of the cleavage (starting after ∼18 min for GE-mix against ∼5 min for GE-control) and also slowed down the enzymatic activity (plateau reached around 90 min for GE-mix against around 60 min for GE-control, see Figure 5) but *in fine*, the enzyme functions with the same yield since 30% of dsR_{43} was cleaved for both mixtures in our experimental conditions. The starting cleavage times obtained from gel electrophoresis analysis are in agreement with the discontinuities of signals in the spectroscopic measurements. The cleavage time is estimated around 90 min for GE-mix from PAGE, in rather good agreement with the time frame for CD signals, which show changes in the time frame between around 70 and 100 min after the addition of the enzyme.

Effect of DNA Length on Supramolecular Assembly with P3HT-PMe_3. To assess the effect of DNA length on the spectroscopic signals, we analyze mixtures of P3HT-PMe_3 with an oligonucleotide dsR_{20} (see Table S1), having a similar sequence and serving as a point of comparison with a number of base pairs in between that of the two fragments (be1 and

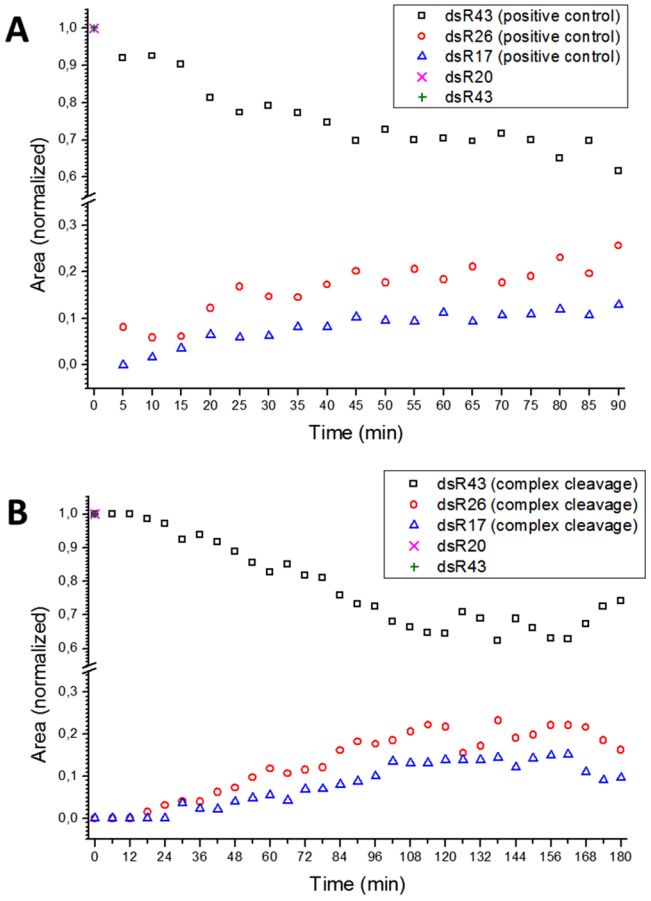

Figure 5. Normalized areas of the intensity peaks of PAGE bands obtained from the enzymatic assays. (A) Enzymatic assay for the control experiment (dsR_{43} + *Hpa*I). (B) Enzymatic assay with cationic polythiophene (dsR_{43}/P3HT-PMe_3 + *Hpa*I).

be2) expected after the cleavage by *Hpa*I. This also allowed us to maintain approximately the same charge ratio in the mixture with P3HT-PMe_3 with respect to mixtures with dsR_{43} (dsR_{20} samples were twice more concentrated than dsR_{43} samples). Solutions dsR_{20} + P3HT-PMe_3 are colored red with a λ_{max} around 510 nm in UV−vis absorption spectra, whereas complexes with dsR_{43} + P3HT-PMe_3 are orange and absorb around 470 nm. For the sake of comparison, CD titration experiment is carried out as for solution with dsR_{43} (Figure S9). A bisignate ICD signal appears with a zero-crossing around 470 nm, and a negative signal around 520 nm. For all molar ratios tested in the titration experiment, this represents a wavelength shift of around $\Delta\lambda = -10$ nm and -5 nm, respectively compared to related CD signals of samples with dsR_{43} with the same molar ratio (Figure 1). This again supports that the changes in the ICD signals upon addition of *Hpa*I enzyme, especially in the wavelengths shifts, are due to the chemical modification of DNA.

To cast light on the origin of the changes in the ICD signals (in the polymer absorption range) upon cleavage of DNA, we carry out MD simulations on each DNA fragment be1 and be2 in interaction with one polymer chain, see MD snapshots in Figure 6. As with the formation of the complex between P3HT-PMe_3 and the longer dsR_{43} DNA, MD simulations show a rapid self-assembly between each DNA fragment and P3HT-PMe_3. The interdistance between the centers of masses of P3HT-PMe_3 and each DNA fragment is rapidly decreasing

DOI: 10.1021/acsabm.9b00123
ACS Appl. Bio Mater. 2019, 2, 2125−2136

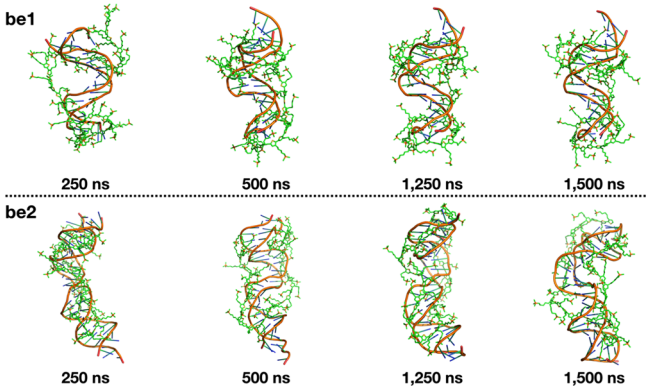

Figure 6. MD snapshots of complexes of P3HT-PMe_3 and DNA fragments be1 (top) or be2 (bottom). The polymer is depicted in green sticks, and cartoon representations were used for DNA (backbones in orange). For clarity, hydrogen atoms of P3HT-PMe_3 were omitted.

during the first 10 ns of the MD simulations, going from ∼10 to 7 Å for the be1 case, and from 16 to 2.2 Å for the be2 case (Figure S10). The small standard deviation of the interdistance profiles (lower than 1 Å for both cases) indicates that there is no dissociation between DNA and P3HT-PMe_3 over the μs time scale. The average interdistance between the center of masses of DNA and polymer is around 4.5 Å for be1 (see distribution on Figure 7A). For the complex with be2, we observe two populations in the distribution of interdistance, due to a reorganization of the polymer at a MD time around 800 ns (Figure S10), with an average at 5.4 Å. In both cases, due to the coiling of the polymer with fragments, the average interdistances are shorter than in the case with dsR43 case (7.8 Å). Regarding the MD snapshots reported in Figure 6, a significant conformational rearrangement of the polymer around the DNA fragments is observed. For complexes with the DNA fragments, the structure of P3HT-PMe_3 polymer are more coiled, wrapped along the DNA helix than in the case with dsR_{43}, for which twisted and relatively linear conformations were encountered.

The profiles of P3HT-PMe_3 end-to-end distances (Figure 7B) have an average of ∼35 and ∼20 Å for the be1 and be2 cases, respectively, versus an average end-to-end distance of 64 Å in the P3HT-PMe_3/dsR_{43} complex (and 180 Å for the fully extended polymer chain). In contrast, the standard deviation of the end-to-end distance can be higher for be1 and be2 cases, i.e., 8.0 and 4.7 Å, respectively, versus 5.2 Å for the dsR_{43} case. The coiling of the polymer around shorter DNAs thus involves a higher degree of flexibility, as also observed with RMSD profiles. The RMSD of the polymer (Figure 7C), when interacting with be1/be2, was therefore large, with an average value of 27 and 25 Å for be1 and be2, respectively, well above the RMSD of P3HT-PMe_3 when it interacts with dsR_{43} (average value ∼15 Å).

From our MD simulations, one can understand that the dynamics of the self-assembly between a DNA and a polymer depends on the DNA length. This is illustrated in Figure 8,

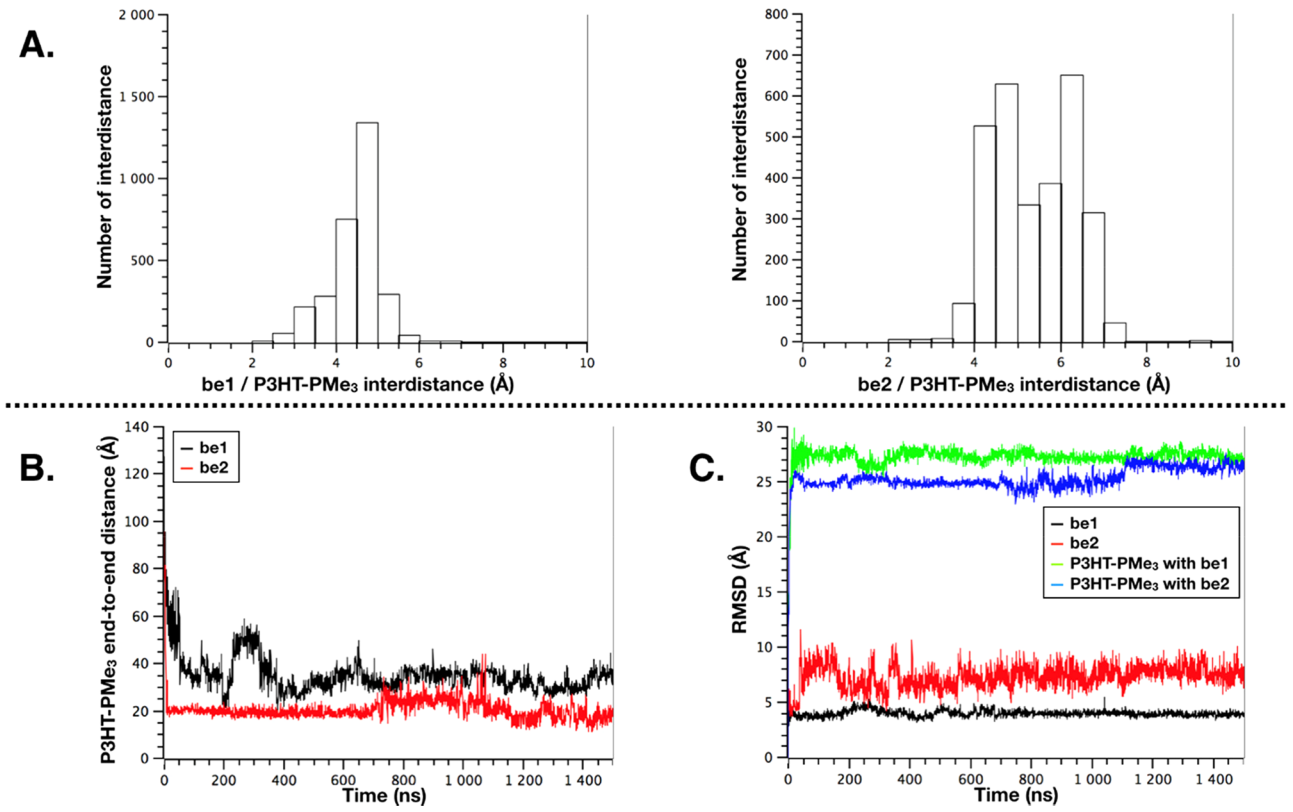

Figure 7. (A) Distribution of interdistances between DNA fragments (be1 or be2) and P3HT-PMe_3 issued from the MD simulations of complexes. The interdistances were calculated according to the center of masses of both partners. (B) End-to-end distance profiles of the P3HT-PMe_3 in complex with be1 (black curve) or be2 (red curve). The end-to-end distances were calculated regarding the first and last sulfur atoms along the polymer sequence. (C) Root-mean-square deviations (RMSD) of components of be1/P3HT-PMe_3 and be2/P3HT-PMe_3 complexes. RMSD were calculated according to the first conformation of the MD production.

DOI: 10.1021/acsabm.9b00123
ACS Appl. Bio Mater. 2019, 2, 2125−2136

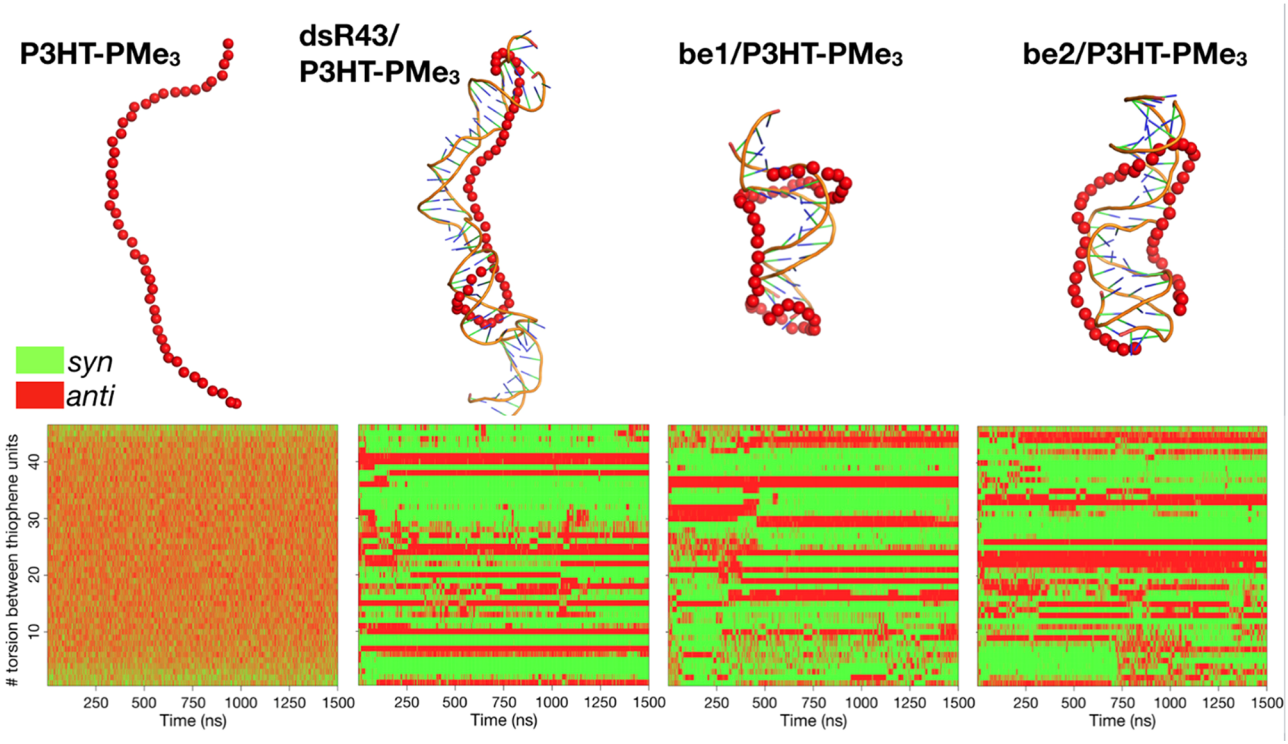

Figure 8. Top: Final MD snapshots (at 1.5 μs) of the pure polymer and DNA/P3HT-PMe$_3$ complexes. The DNA fragments are depicted in cartoon representation (backbones in orange; bases in green/blue sticks). The polymer (red) is depicted in low resolution, each red particle being a thiophene unit centered on the sulfur atom. Bottom: Evolution of the position of syn/anti conformations along the polymer backbone with MD time, for each corresponding system shown on top.

showing the final MD snapshots at a low resolution, showing the different organizations of the polymer according to the DNA fragment. In the case of the longer DNA (dsR$_{43}$), the polymer is more linear, with some coiling around the DNA helix at the ends of the polymer chain. Such an organization allows us to maximize electrostatic interactions between the DNA phosphates and the cationic groups of the polymer. In this case, the polymer shows a longer end-to-end distance with a more static behavior (small RMSD), whereas DNA has an important flexibility associated with a curvature effect. With the smaller DNA fragments, we observe a contrasting situation: the polymer is largely coiled around the DNA. The polymer adopts a more globular shape (smaller end-to-end distance) along with a more flexible behavior (larger RMSD). In parallel, the smaller the DNA fragment, the less important the flexibility of the DNA as it cannot accommodate entirely a long polymer in a linear way. In this sense, we do not observe large curvature conformational effects for the be1 and be2 DNA fragments. The difference between the RMSD of the DNA and the polymer (ΔRMSD in Figure S11) is an indicator of the various levels of conformational changes and flexibility. The ΔRMSD for the dsR$_{43}$ is positive as the long DNA fragment undergoes large conformational changes associated with a higher level of flexibility, whereas the polymer is less flexible, with a rather linear conformation. In contrast, the ΔRMSD for the be1 and be2 systems was negative. In these cases, the polymer adopts large conformational changes and higher level of flexibility, whereas the DNA fragments are more rigid. However, the coiling of the polymer around the DNA leads to restrictions in the conformational freedom in comparison to the pure polymer. Along the MD simulations, we calculated the S−C−C−S dihedral angle between the thiophene units along the polythiophene backbone as an indicator of the coiling (Table S3). For the pure polymer (without DNA), the ratio of the syn/anti is around 45/55 (on 3000 frames over 1.5 μs). This ratio is inverted up to a ratio around 65/35 syn/anti when the polymer was complexed with the DNA fragments. Moreover, the level of syn-periplanar in be1/P3HT-PMe$_3$ is around 10% of the total amount of syn conformations, although it is only around 3% in the case of the pure polymer. Altogether, this shows that the helical structuration of the polymer when it binds to DNA occurs via the reorganization of its backbone toward a stronger syn character between the thiophene units. Remarkably, we observe that the syn/anti character is not distributed randomly along the polymer chain when it is complexed with DNA, as depicted by graphs in Figure 8 bottom for each MD system on top. In those graphs, we plot the position of syn (green) and anti (red) conformations between successive thiophene units along the polymer chain, as a function of the MD time. For the pure polymer (bottom left), we observe that changes from anti/syn occurred randomly along the sequence with time. In contrast, for DNA/polymer complexes, there are portions of pure syn (green) and of pure anti (red) that are preserved throughout time. These graphs show that the coiling of the polymer chain occurred by rather large portions of neighboring syn conformations, extending from a few thiophene units up to around ten thiophene units, separated by rather small portions of anti conformations.

The calculated CD spectra, averaged either over a few (5) selected polymer conformations at the semiempirical INDO/SCI level (Figure S12) or over all frames saved after 1 μs of simulation time using a simplified excitonic model (Figure 9A),[63] yield (−/+) CD signals, in fair agreement with the

DOI: 10.1021/acsabm.9b00123
ACS Appl. Bio Mater. 2019, 2, 2125−2136

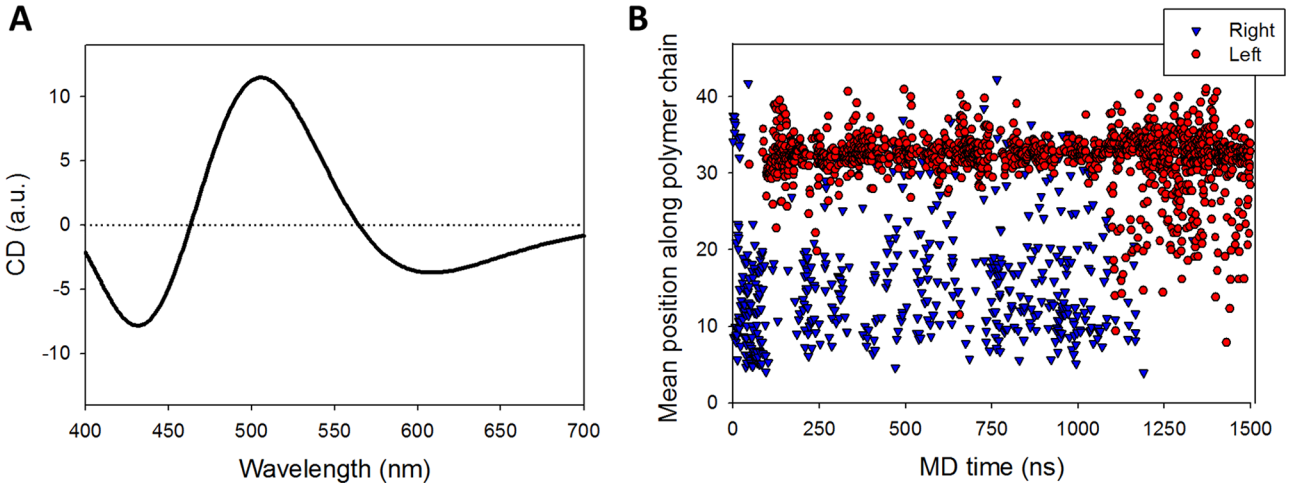

Figure 9. (A) Calculated CD spectra of the polythiophene chain in the dsR_{43}/P3HT-PMe_3 complex using a simplified excitonic model, as averaged over 1000 frames between 1.0 and 1.5 μs of the MD simulations. B. Position (in the number of thiophene unit along the polythiophene chain) of the exciton states contributing to the low-energy part of the CD response (left helicity in red, right helicity in blue) as a function of the MD time.

experimental CD spectra in Figure 1. The coupled MD/excitonic simulations reveal a rather rich dynamical behavior, with rapid switching between left-handed and right-handed arrangements preceding a stable phase where left-handed ((−/+) CD signals) conformations are largely preferred, Figure 9B.

From the detailed wave function analysis of the exciton states contributing to the low-energy part of the CD response reported in Figure 9B, one can clearly correlate the preferential left helicity to the formation of an extended, mostly *syn* domain (located on the second half of the polymer backbone, around residue 35). It is the concerted motion of the monomer units toward successive syn linkages, likely driven by electrostatic interactions with the DNA double strand (which more than compensate the syn−anti torsion energy penalty), that triggers the (left) chiral induction of the polymer backbone. We stress that the need for concerted twisting of the side-chain equipped monomers also explains why long MD simulation runs are required to stabilize the left helix in dsR_{43}. Though further investigations are required, we tentatively propose that the reduced polymer CD signal recorded for the mixture of be1 and be2 is because of the (slightly) smaller syn domains achieved using these shorter templates (Figure 8). Finally, it is worth pointing out that the lowest exciton energies, as probed e.g. from the first zero-crossing point on the CD curves, are expected to be shifted toward higher wavelengths when going from random to concerted sequences of torsion angles, as typically encountered in situations where disorder is spatially correlated. This holds true in the case at hands here, as evident from Figure 3D.

CONCLUSIONS

We have used a supramolecular approach for a continuous readout of the activity of an endonuclease enzyme toward DNA. By utilizing an achiral cationic π-conjugated polymer that interacts with DNA and the effects of chiral induction from the DNA to the polymer, we have probed the modifications of the DNA structure in real-time through UV−vis and CD spectroscopies. In the experimental conditions used for this study, the enzymatic activity, as explored by the ICD signals, occurred within a time frame of 70−100 min. This is in agreement with the results of a noncontinuous assay by polyacrylamide gel electrophoresis, for which we estimated a time of around 90 min to reach a maximum cleavage rate of 30% DNA in our experimental conditions. This illustrates the sensitivity of induced CD signals to probe in real-time the changes in the nucleic acid structure when it interacts with a π-conjugated polymer. Although the π-conjugated polymer interacts strongly with the DNA, it only hinders the enzymatic activity to a low extent (for a cleavage rate of 30%, ∼90 min with the polymer instead of ∼60 min without the polymer). However, further work has to be carried out to relate in detail the changes observed in the ICD signals with time to the kinetic parameters of the enzymatic activity. By combining MD simulations and calculations of CD spectra, we clarified the left-handed helical conformations of the polymer when it interacts with DNA, together with the effect of DNA length on the organization and the dynamics within the complex. Altogether, this study may help further development of a continuous approach to monitor of enzymatic activity based on chiroptical spectroscopy signals of dynamic supramolecular assemblies. This is potentially applicable to other types of enzymes catalyzing reactions with genetic material, for instance, methyltransferases, as the addition of methyl groups on nucleobases modifies the 3D structure of DNA.

ASSOCIATED CONTENT

Supporting Information

The Supporting Information is available free of charge on the ACS Publications website at DOI: 10.1021/acsabm.9b00123.

Additional spectra, graphs, theoretical details, and modeling data (PDF)

AUTHOR INFORMATION

Corresponding Author

*Email: mathieu.surin@umons.ac.be.

ORCID

Sébastien Clément: 0000-0002-8473-8197

Mathieu Surin: 0000-0001-8950-3437

DOI: 10.1021/acsabm.9b00123
ACS Appl. Bio Mater. 2019, 2, 2125−2136

Author Contributions

†M.F. and M.E.T. contributed equally. The manuscript was written through the contribution of all authors. All authors have given approval to the final version of the manuscript.

Notes

The authors declare no competing financial interest.

■ ACKNOWLEDGMENTS

Research in Mons was supported by the Fund for Scientific Research (F.R.S.-FNRS) under Grants MIS F.4532.16 (SHERPA) and EOS 30650939 (PRECISION). Computational resources have been provided by the Consortium des Équipements de Calcul Intensif (CÉCI), funded by the F.R.S.-FNRS under Grant 2.5020.11. V.C., D.B,. and M.S. are F.R.S.-FNRS researchers. Research in Montpellier is supported by CNRS and Université de Montpellier.

■ REFERENCES

(1) Turner, A. P. F. Biosensors: Sense and Sensibility. *Chem. Soc. Rev.* **2013**, *42*, 3184−3196.
(2) Wu, Y.; Tilley, R. D.; Gooding, J. Challenges and Solutions in Developing Ultrasensitive Biosensors. *J. Am. Chem. Soc.* **2019**, *141*, 1162−1170.
(3) Wang, X.; Lu, X.; Chen, J. Development of Biosensor Technologies for Analysis of Environmental Contaminants. *Trends Environ. Anal. Chem.* **2014**, *2*, 25−32.
(4) Mittal, S.; Kaur, H.; Gautam, N.; Mantha, A. K. Biosensors for Breast Cancer Diagnosis: A Review of Bioreceptors, Biotransducers and Signal Amplification Strategies. *Biosens. Bioelectron.* **2017**, *88*, 217−231.
(5) Rotariu, L.; Lagarde, F.; Jaffrezic-Renault, N.; Bala, C. Electrochemical Biosensors for Fast Detection of Food Contaminants − Trends and Perspective. *TrAC, Trends Anal. Chem.* **2016**, *79*, 80−87.
(6) Nilsson, K. P. R.; Aslund, A.; Berg, I.; Nyström, S.; Konradsson, P.; Herland, A.; Inganäs, O.; Stabo-Eeg, F.; Lindgren, M.; Westermark, G. T.; Lannfelt, L.; Nilsson, L. N.; Hammarström, P. Imaging Distinct Conformational States of Amyloid-beta Fibrils in Alzheimer's Disease using Novel Luminescent Probes. *ACS Chem. Biol.* **2007**, *2*, 553−560.
(7) Bajaj, A.; Miranda, O. R.; Phillips, R.; Kim, I. B.; Jerry, D. J.; Bunz, U. H. F.; Rotello, V. M. Array-based Sensing of Normal, Cancerous, and Metastatic Cells using Conjugated Fluorescent Polymers. *J. Am. Chem. Soc.* **2010**, *132*, 1018−1022.
(8) Duan, X.; Liu, L.; Feng, F.; Wang, S. Cationic Conjugated Polymers for Optical Detection of DNA methylation, Lesions, and Single Nucleotide Polymorphisms. *Acc. Chem. Res.* **2010**, *43*, 260−270.
(9) Doré, K.; Dubus, S.; Ho, H.-A.; Lévesque, I.; Brunette, M.; Corbeil, G.; Boissinot, M.; Boivin, G.; Bergeron, M. G.; Boudreau, D.; Leclerc, M. Fluorescent Polymeric Transducer for the Rapid, Simple, and Specific Detection of Nucleic Acids at the Zeptomole Level. *J. Am. Chem. Soc.* **2004**, *126*, 4240−4244.
(10) Lubin, A. A.; Lai, R. Y.; Baker, B. R.; Heeger, A. J.; Plaxco, K. W. Sequence-specific, Electronic Detection of Oligonucleotides in Blood, Soil, and Foodstuffs with the Reagentless, Reusable E-DNA sensor. *Anal. Chem.* **2006**, *78*, 5671−5677.
(11) Chi, C.; Mikhailovsky, A.; Bazan, G. C. Design of Cationic Conjugated Polyelectrolytes for DNA Concentration Determination. *J. Am. Chem. Soc.* **2007**, *129*, 11134−11145.
(12) Malygin, E. G.; Hattman, S. DNA Methyltransferases: Mechanistic Models derived from Kinetic Analysis. *Crit. Rev. Biochem. Mol. Biol.* **2012**, *47*, 97−193.
(13) Hickman, A. B.; Dyda, F. DNA Transposition at Work. *Chem. Rev.* **2016**, *116*, 12758−12784.
(14) Wan, L.; Chen, Q.; Liu, J.; Yang, X.; Huang, J.; Li, L.; Guo, X.; Zhang, J.; Wang, K. Programmable Self-Assembly of DNA−Protein Hybrid Hydrogel for Enzyme Encapsulation with Enhanced Biological Stability. *Biomacromolecules* **2016**, *17*, 1543−1550.
(15) Zelzer, M.; Todd, S. J.; Hirst, A. R.; McDonald, T. O.; Ulijn, R. V. Enzyme-Responsive Materials: Design Strategies and Future Developments. *Biomater. Sci.* **2013**, *1*, 11−39.
(16) Hirst, A. R.; Escuder, B.; Miravet, J. F.; Smith, D. K. High-tech Applications of Self-Assembling Supramolecular Nanostructured Gel-phase Materials: from Regenerative Medicine to Electronic Devices. *Angew. Chem., Int. Ed.* **2008**, *47*, 8002−8018.
(17) Ishino, S.; Ishino, Y. DNA Polymerases as Useful Reagents for Biotechnology - the History of Developmental Research in the Field. *Front. Microbiol.* **2014**, *5* (465), 1−8.
(18) Loenen, W. A. M.; Dryden, D. T. F.; Raleigh, E. A.; Wilson, G. G.; Murray, N. E. Highlights of the DNA Cutters: a Short History of the Restriction Enzymes. *Nucleic Acids Res.* **2014**, *42*, 3−19.
(19) Breaker, R. R. DNA Enzymes. *Nat. Biotechnol.* **1997**, *15*, 427−431.
(20) Pingoud, A.; Jeltsch, A.; Maxwell, A.; Sherratt, D. Enzymes that keep DNA under Control. *EMBO Rep.* **2001**, *2*, 271−276.
(21) *Fundamental of Enzyme Kinetics*, 4th ed.; Cornish-Bowden, A., Ed.; Wiley−VCH, 2012.
(22) Johnson, K. A. A Century of Enzyme Kinetic Analysis, 1913 to 2013. *FEBS Lett.* **2013**, *587*, 2753−2766.
(23) Dai, N.; Kool, E. T. Fluorescent DNA-based Enzyme Sensors. *Chem. Soc. Rev.* **2011**, *40*, 5756−5770.
(24) Juskowiak, B. Nucleic Acid-based Fluorescent Probes and their Analytical Potential. *Anal. Bioanal. Chem.* **2011**, *399*, 3157−3176.
(25) Wang, D.; Gong, X.; Heeger, P. S.; Rininsland, F.; Bazan, G. C.; Heeger, A. J. Biosensors from Conjugated Polyelectrolyte Complexes. *Proc. Natl. Acad. Sci. U. S. A.* **2002**, *99*, 49−53.
(26) Surin, M. From Nucleobase to DNA Templates for Precision Supramolecular Assemblies and Synthetic Polymers. *Polym. Chem.* **2016**, *7*, 4137−4150.
(27) Gaylord, B. S.; Heeger, A. J.; Bazan, G. C. DNA Detection using Water-soluble Conjugated Polymers and Peptide Nucleic Acid Probes. *Proc. Natl. Acad. Sci. U. S. A.* **2002**, *99*, 10954−10957.
(28) Nilsson, K. P. R.; Inganäs, O. Chip and Solution Detection of DNA Hybridization using a Luminescent Zwitterionic Polythiophene Derivative. *Nat. Mater.* **2003**, *2*, 419−424.
(29) Ho, H.-A.; Najari, A.; Leclerc, M. Optical Detection of DNA and Proteins with Cationic Polythiophenes. *Acc. Chem. Res.* **2008**, *41*, 168−178.
(30) Feng, X.; Liu, L.; Wang, S.; Zhu, D. Water-soluble Fluorescent Conjugated Polymers and their Interactions with Biomacromolecules for Sensitive Biosensors. *Chem. Soc. Rev.* **2010**, *39*, 2411−2419.
(31) Zhu, C.; Liu, L.; Yang, Q.; Lv, F.; Wang, S. Water-Soluble Conjugated Polymers for Imaging, Diagnosis, and Therapy. *Chem. Rev.* **2012**, *112*, 4687−4735.
(32) Rajwar, D.; Ammanath, G.; Cheema, J. A.; Palaniappan, A.; Yildiz, U. H.; Liedberg, B. Tailoring Conformation-Induced Chromism of Polythiophene Copolymers for Nucleic Acid Assay at Resource Limited Settings. *ACS Appl. Mater. Interfaces* **2016**, *8*, 8349−8357.
(33) Wang, Y.; Schanze, K. S.; Chi, E. Y.; Whitten, D. G. When Worlds Collide: Interactions at the Interface between Biological Systems and Synthetic Cationic Conjugated Polyelectrolytes and Oligomers. *Langmuir* **2013**, *29*, 10635−10647.
(34) Knoops, J.; Rubio-Magnieto, J.; Richeter, S.; Clément, S.; Surin, M., Supramolecular Assemblies of DNA/Conjugated Polymers. *Conjugated Polymers and Oligomers: Structural and Soft Matter Aspects*; Knaapila, M., Ed.; World Scientific Publishing, 2018; Vol. *9*, Chapter 5, pp 139−157.
(35) Kaloni, T. P.; Giesbrecht, P. K.; Schreckenbach, G.; Freund, M. S. Polythiophene: From Fundamental Perspectives to Applications. *Chem. Mater.* **2017**, *29*, 10248−10283.
(36) Das, S.; Routh, P.; Ghosh, R.; Chatterjee, D. P.; Nandi, A. K. Water-soluble Ionic Polythiophenes for Biological and Analytical Applications. *Polym. Int.* **2017**, *66*, 623−639.

DOI: 10.1021/acsabm.9b00123
ACS Appl. Bio Mater. 2019, 2, 2125−2136

(37) Gaylord, B. S.; Massie, M. R.; Feinstein, S. C.; Bazan, G. C. SNP Detection using Peptide Nucleic Acid Probes and Conjugated Polymers: Applications in Neurodegenerative Disease Identification. *Proc. Natl. Acad. Sci. U. S. A.* **2005**, *102*, 34−39.
(38) Liu, Z.; Wang, H.-L.; Cotlet, M. Energy Transfer from a Cationic Conjugated Polyelectrolyte to a DNA Photonic Wire: Toward Label-Free, Sequence-Specific DNA Sensing. *Chem. Mater.* **2014**, *26*, 2900−2906.
(39) (a) Tang, Y.; Feng, F.; He, F.; Wang, S.; Li, Y.; Zhu, D. Direct Visualization of Enzymatic Cleavage and Oxidative Damage by Hydroxyl Radicals of Single-Stranded DNA with a Cationic Polythiophene Derivative. *J. Am. Chem. Soc.* **2006**, *128*, 14972−14976.
(40) Feng, F.; Liu, L.; Yang, Q.; Wang, S. Water-soluble Conjugated Polymers for Fluorescent-Enzyme Assays. *Macromol. Rapid Commun.* **2010**, *31*, 1405−1421.
(41) Lian, S.; Liu, C.; Zhang, X.; Wang, H.; Li, Z. Detection of T4 Polynucleotide Kinase Activity based on Cationic Conjugated Polymer-mediated Fluorescence Resonance Energy Transfer. *Biosens. Bioelectron.* **2015**, *66*, 316−320.
(42) Yang, Q.; Dong, Y.; Wu, W.; Zhu, C.; Chong, H.; Lu, J.; Yu, D.; Liu, L.; Lv, F.; Wang, S. Detection and Differential Diagnosis of Colon Cancer by a Cumulative Analysis of Promoter Methylation. *Nat. Commun.* **2012**, *3*, 1206.
(43) Feng, F.; Wang, H.; Han, L.; Wang, S. Fluorescent Conjugated Polyelectrolyte as an Indicator for Convenient Detection of DNA Methylation. *J. Am. Chem. Soc.* **2008**, *130*, 11338−11343.
(44) Kumar, M.; Brocorens, P.; Tonnelé, C.; Beljonne, D.; Surin, M.; George, S. J. A Dynamic Supramolecular Polymer with Stimuli-Responsive Handedness for in situ Probing of Enzymatic ATP hydrolysis. *Nat. Commun.* **2014**, *5*, 5793.
(45) Pescitelli, G.; Di Bari, L.; Berova, N. Application of Electronic Circular Dichroism in the Study of Supramolecular Systems. *Chem. Soc. Rev.* **2014**, *43*, 5211−5233.
(46) Liu, M.; Zhang, L.; Wang, T. Supramolecular Chirality in Self-Assembled Systems. *Chem. Rev.* **2015**, *115*, 7304−7397.
(47) Balaz, M.; Tannir, S.; Varga, K. Chiral Multichromophoric Supramolecular Nanostructures Assembled by single stranded DNA and RNA Templates. *Coord. Chem. Rev.* **2017**, *349*, 66−83.
(48) Holmgaard List, N.; Knoops, J.; Rubio-Magnieto, J.; Idé, J.; Beljonne, D.; Norman, P.; Surin, M.; Linares, M. Origin of DNA-induced Circular Dichroism in a Minor-Groove Binder. *J. Am. Chem. Soc.* **2017**, *139*, 14947−14953.
(49) Rubio-Magnieto, J.; Phan, T. A.; Fossepré, M.; Matot, V.; Knoops, J.; Jarrosson, T.; Dumy, P.; Serein-Spirau, F.; Niebel, C.; Ulrich, S.; Surin, M. Photomodulation of DNA-Templated Supramolecular Assemblies. *Chem. - Eur. J.* **2018**, *24*, 706−714.
(50) Rubio-Magnieto, J.; Azene, E. G.; Knoops, J.; Knippenberg, S.; Delcourt, C.; Thomas, A.; Richeter, S.; Mehdi, A.; Dubois, Ph.; Lazzaroni, R.; Beljonne, D.; Clément, S.; Surin, M. Self-assembly and hybridization mechanisms of DNA with cationic polythiophene. *Soft Matter* **2015**, *11*, 6460−6471.
(51) Rubio-Magnieto, J.; Thomas, A.; Richeter, S.; Mehdi, A.; Dubois, Ph; Lazzaroni, R.; Clément, S.; Surin, M. Chirality in DNA − π-conjugated polymer supramolecular structures: insights into the self-assembly. *Chem. Commun.* **2013**, *49*, 5483−5485.
(52) Modrich, P. Structures and Mechanisms of DNA Restriction and Modification Enzymes. *Q. Rev. Biophys.* **1979**, *12*, 315−369.
(53) Clément, S.; Tizit, A.; Desbief, S.; Mehdi, A.; De Winter, J.; Gerbaux, P.; Lazzaroni, R.; Boury, B. Synthesis and Characterisation of π-Conjugated Polymer/Silica Hybrids Containing Regioregular Ionic Polythiophenes. *J. Mater. Chem.* **2011**, *21*, 2733−2739.
(54) Case, D. A.; Cheatham, T. E., III; Darden, T.; Gohlke, H.; Luo, R.; Merz Jr, K.; Onufriev, A.; Simmerling, C.; Wang, B.; Woods, R. J. The AMBER Biomolecular Simulation Programs. *J. Comput. Chem.* **2005**, *26*, 1668−1688.
(55) Ivani, I.; Dans, P. D.; Noy, A.; Pérez, A.; Faustino, I.; Hospital, A.; Walther, J.; Andrio, P.; Goni, R.; Balaceanu, A.; Portella, G.; Battistini, F.; Gelpi, J. L.; Gonzales, C.; Vendruscolo, M.; Laughton, C. A.; Harris, S. A.; Case, D. A.; Orozco, M. Parmbsc1: a Refined Force Field for DNA Simulations. *Nat. Methods* **2016**, *13*, 55−58.
(56) Wang, J.; Wolf, R. M.; Caldwell, J. W.; Kollman, P. A.; Case, D. A. Development and Testing of a General AMBER Force Field. *J. Comput. Chem.* **2004**, *25*, 1157−1174.
(57) Hawkins, G.; Cramer, C.; Truhlar, D. Pairwise Solute Descreening of Solute Charges from a Dielectric Medium. *Chem. Phys. Lett.* **1995**, *246*, 122−129.
(58) R Core Team. *R*; R Foundation for Statistical Computing: Vienna, Austria, 2013; www.R-project.org.
(59) *The Pymol Molecular Graphics System*, version 2.0; Schrödinger LLC; www.pymol.org.
(60) Sjöqvist, J.; Maria, J.; Simon, R. A.; Linares, M.; Norman, P.; Nilsson, K. P. R.; Lindgren, M. Toward a Molecular Understanding of the Detection of Amyloid Proteins with Flexible Conjugated Oligothiophenes. *J. Phys. Chem. A* **2014**, *118*, 9820−9827.
(61) Selegård, R.; Rouhbakhsh, Z.; Shirani, H.; Johansson, L. B. G.; Norman, P.; Linares, M.; Aili, D.; Nilsson, K. P. R. Distinct Electrostatic Interactions Govern the Chiro-Optical Properties and Architectural Arrangement of Peptide-Oligothiophene Hybrid Materials. *Macromolecules* **2017**, *50*, 7102−7110.
(62) König, C.; Skanberg, R.; Hotz, I.; Ynnerman, A.; Norman, P.; Linares, M. Binding Sites for Luminescent Amyloid Biomarkers from non-Biased Molecular Dynamics Simulations. *Chem. Commun.* **2018**, *54*, 3030−3033.
(63) Lin, J.; Surin, M.; Beljonne, D.; Lou, X.; van Dongen, J. L. J.; Schenning, A. P. H. J. On the Mechanism of Dynamic Polymerization via Recycled ssDNA Templated Assembly of Non-Natural Bases. *Chem. Sci.* **2012**, *3*, 2732−2736.

DOI: 10.1021/acsabm.9b00123
ACS Appl. Bio Mater. 2019, 2, 2125−2136